

## **Supplementary Information**

### **An asymmetric Sodium Extraction/Insertion Mechanism for the Fe/V-mixed NASICON $\text{Na}_4\text{FeV}(\text{PO}_4)_3$**

Sunkyu Park <sup>1,2,3</sup>, Jean-Noël Chotard <sup>1,5</sup>, Dany Carlier <sup>2,5</sup>, Iona Moog <sup>3</sup>, Mathieu Duttine <sup>2</sup>, François Fauth <sup>4</sup>, Antonella Iadecola <sup>5</sup>, Laurence Croguennec <sup>\*,2,5</sup> and Christian Masquelier <sup>\*,1,5</sup>

<sup>1</sup> *Laboratoire de Réactivité et de Chimie des Solides, Université de Picardie Jules Verne,*

*CNRS-UMR 7314, F-80039 Amiens Cedex 1, France*

<sup>2</sup> *CNRS, Univ. Bordeaux, Bordeaux INP, ICMCB UMR 5026, F-33600 Pessac,  
France*

<sup>3</sup> *TIAMAT, 15 Rue Baudelocque, 80000 Amiens*

<sup>4</sup> *CELLS-ALBA Synchrotron, Cerdanyola del Vallès, E-08290 Barcelona, Spain*

<sup>5</sup> *RS2E, Réseau sur le stockage électrochimique de l'énergie, FR CNRS 3459,  
F-80039 Amiens Cedex 1, France*

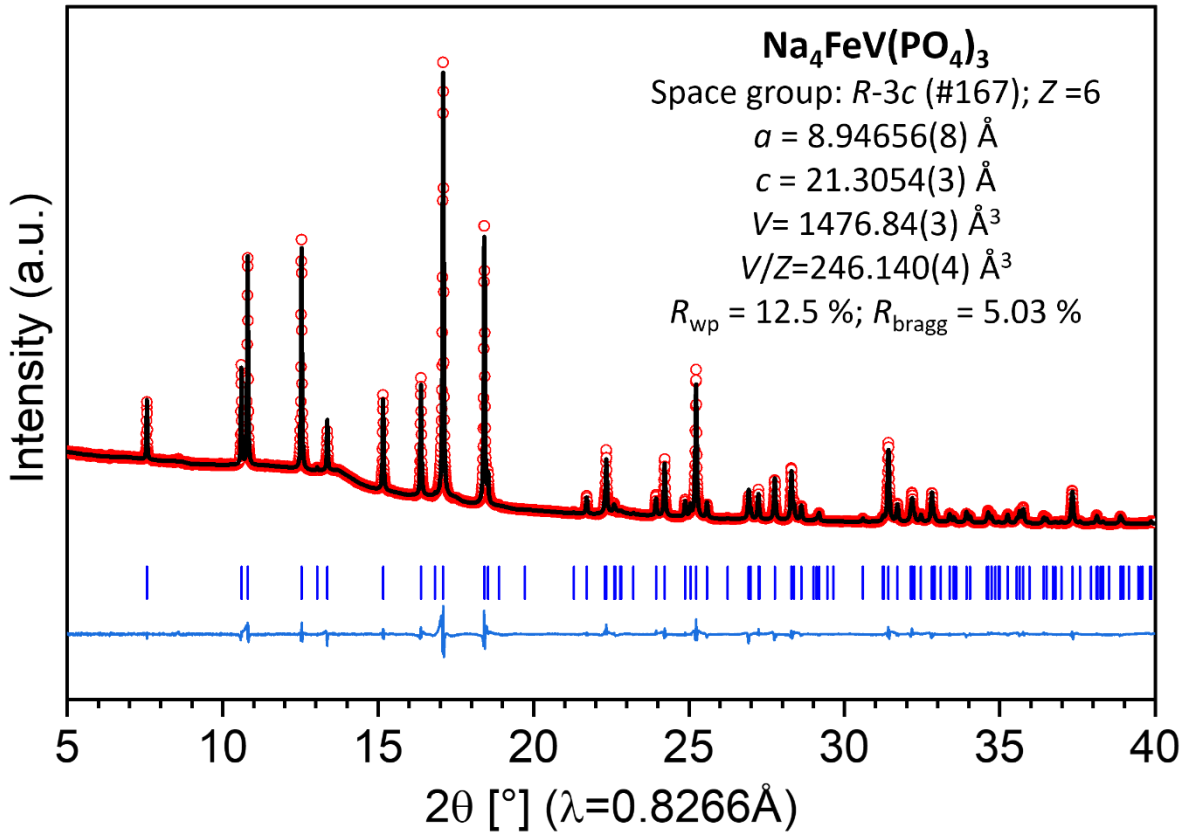


**Figure S1.** Rietveld refinement results of the pre-sodiated  $\text{Na}_4\text{FeV}(\text{PO}_4)_3$  powder collected within a capillary at 298 K.

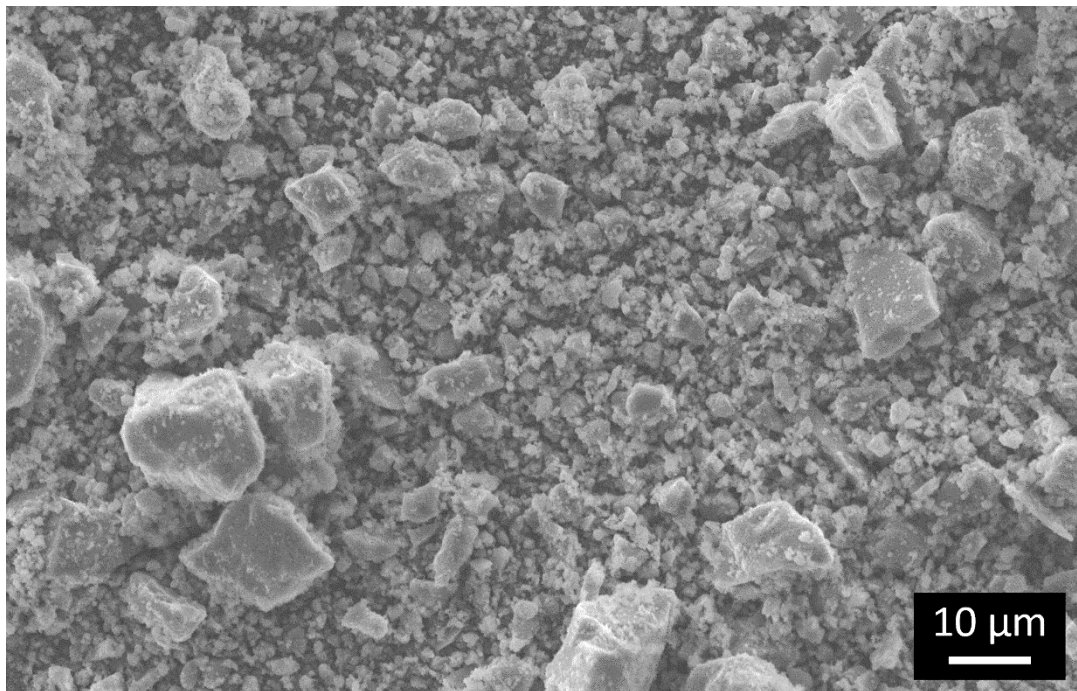


**Figure S2.** SEM image of the as-prepared  $\text{Na}_3\text{FeV}(\text{PO}_4)_3$  powder.

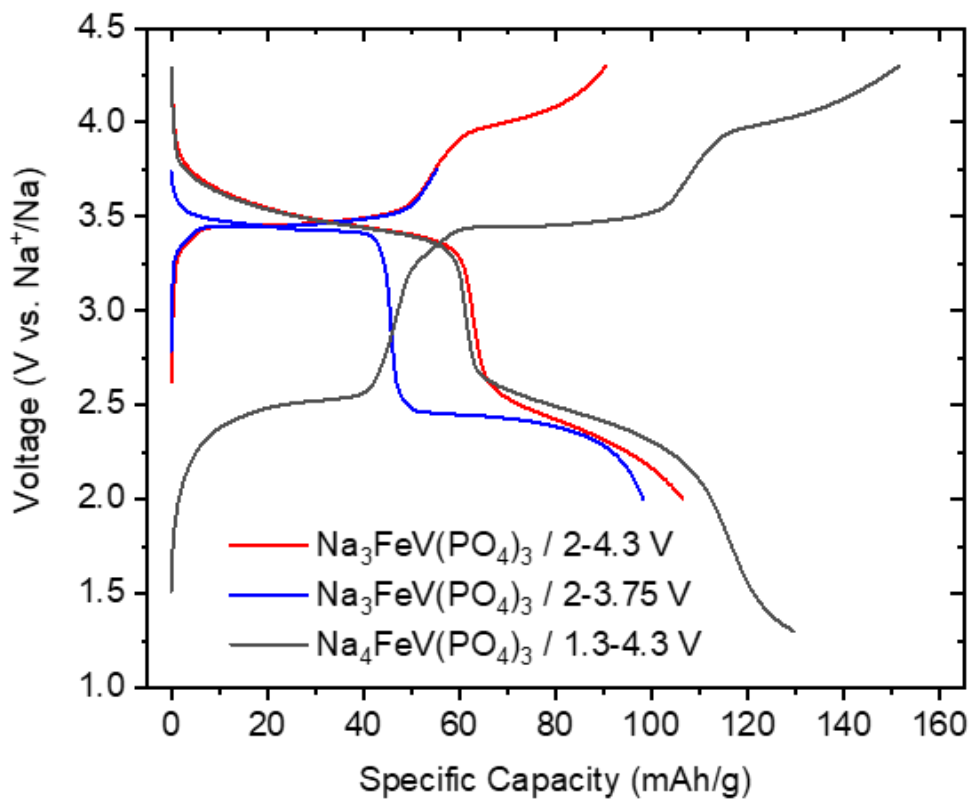


**Figure S3.** Electrochemical charge and discharge curves of the as-prepared  $\text{Na}_3\text{FeV}(\text{PO}_4)_3$  within the two voltage windows of 2-3.75 V and 2-4.3 V and the pre-sodiated  $\text{Na}_4\text{FeV}(\text{PO}_4)_3$  within the voltage window of 1.3-4.3 V with a C-rate of C/15 (1  $\text{Na}^+$  in 15 h).

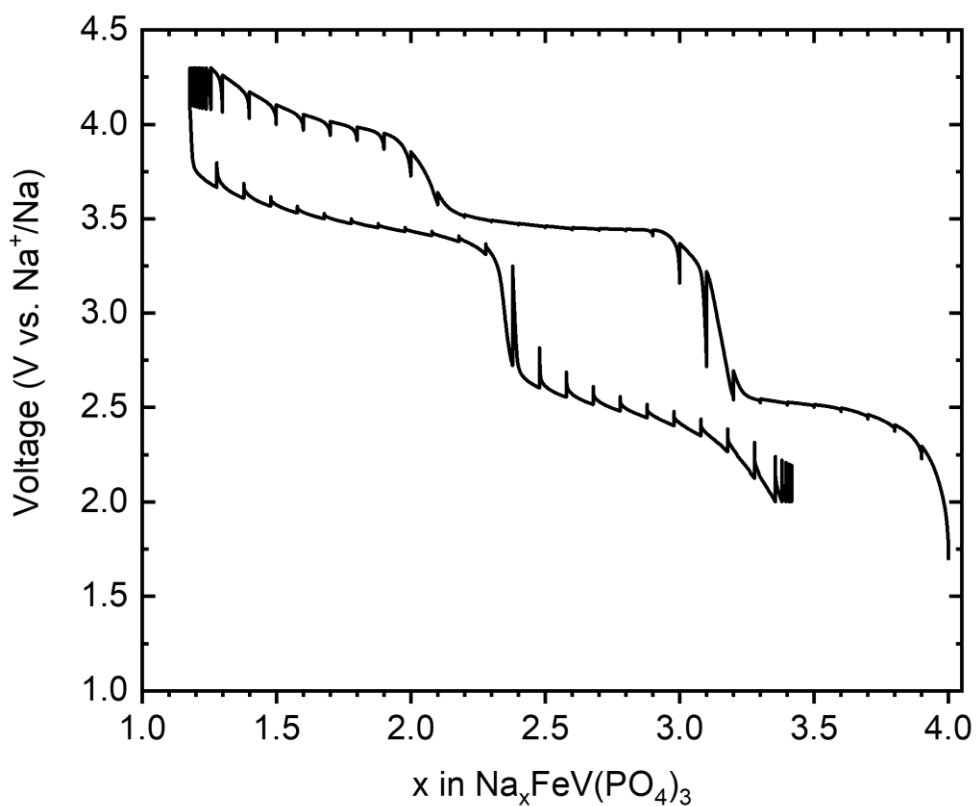


**Figure S4.** Quasi-galvanostatic intermittent titration technique (GITT) curve for the first charge up to 4.3 V vs. Na<sup>+</sup>/Na and discharge down to 2.0 V vs. Na<sup>+</sup>/Na of the pre-sodiated Na<sub>4</sub>FeV(PO<sub>4</sub>)<sub>3</sub> electrode material when applying a voltage step for 2 h at a C-rate of C/20/ion followed by 4 h of relaxation after each voltage step.

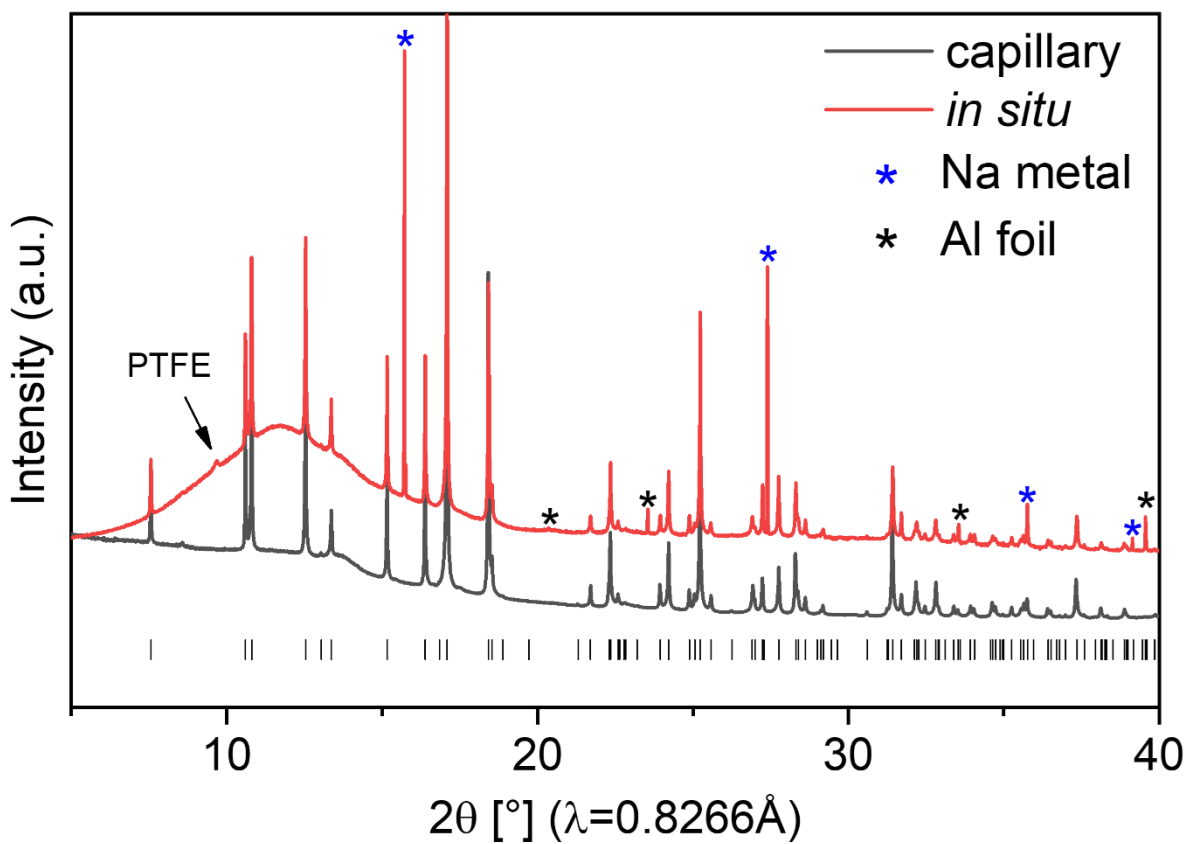


**Figure S5.** Comparison of the synchrotron SRPD patterns collected *ex situ* in a capillary and *in situ* in the electrochemical cell (just before starting the experiment) for the pristine pre-sodiated  $\text{Na}_4\text{FeV}(\text{PO}_4)_3$  electrode material.

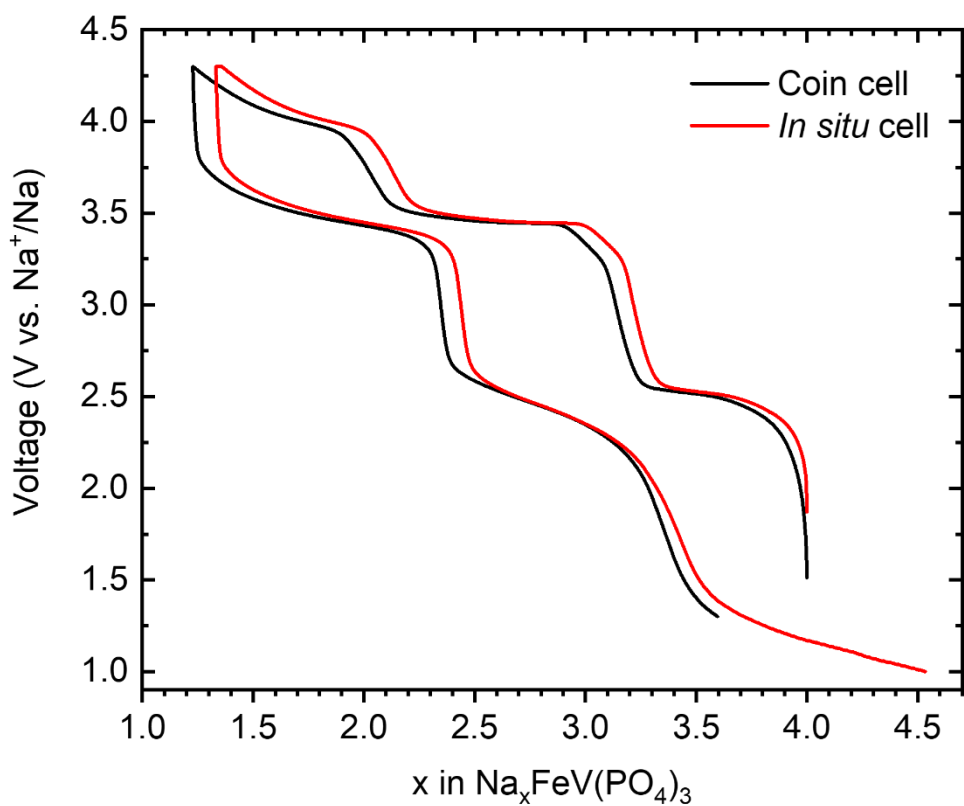


**Figure S6.** Electrochemical charge and discharge curves obtained for the pre-sodiated  $\text{Na}_4\text{FeV}(\text{PO}_4)_3$  electrode material when cycled vs. Na metal, in a normal coin cell and in the *in situ* cell.

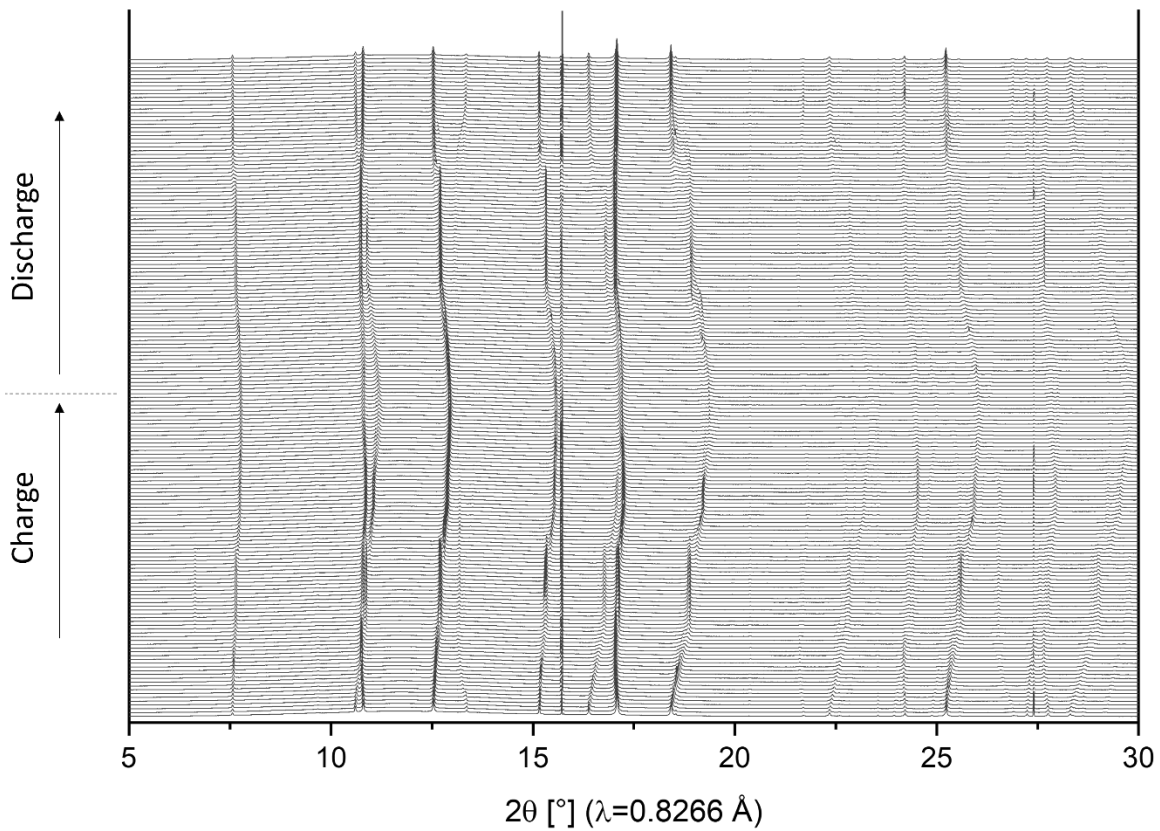


**Figure S7.** Wider  $2\theta$  range synchrotron XRPD patterns collected *operando* during the first cycle of  $\text{Na}_4\text{FeV}(\text{PO}_4)_3$  vs. Na metal, within a voltage window of 1.0 – 4.3 V vs.  $\text{Na}^+/\text{Na}$  at the C-rate of C/15 (= 1  $\text{Na}^+$  in 15 h). The same data including the counter plot with the narrower  $2\theta$  range of 6.5 – 13.2° are shown in Figure 3.

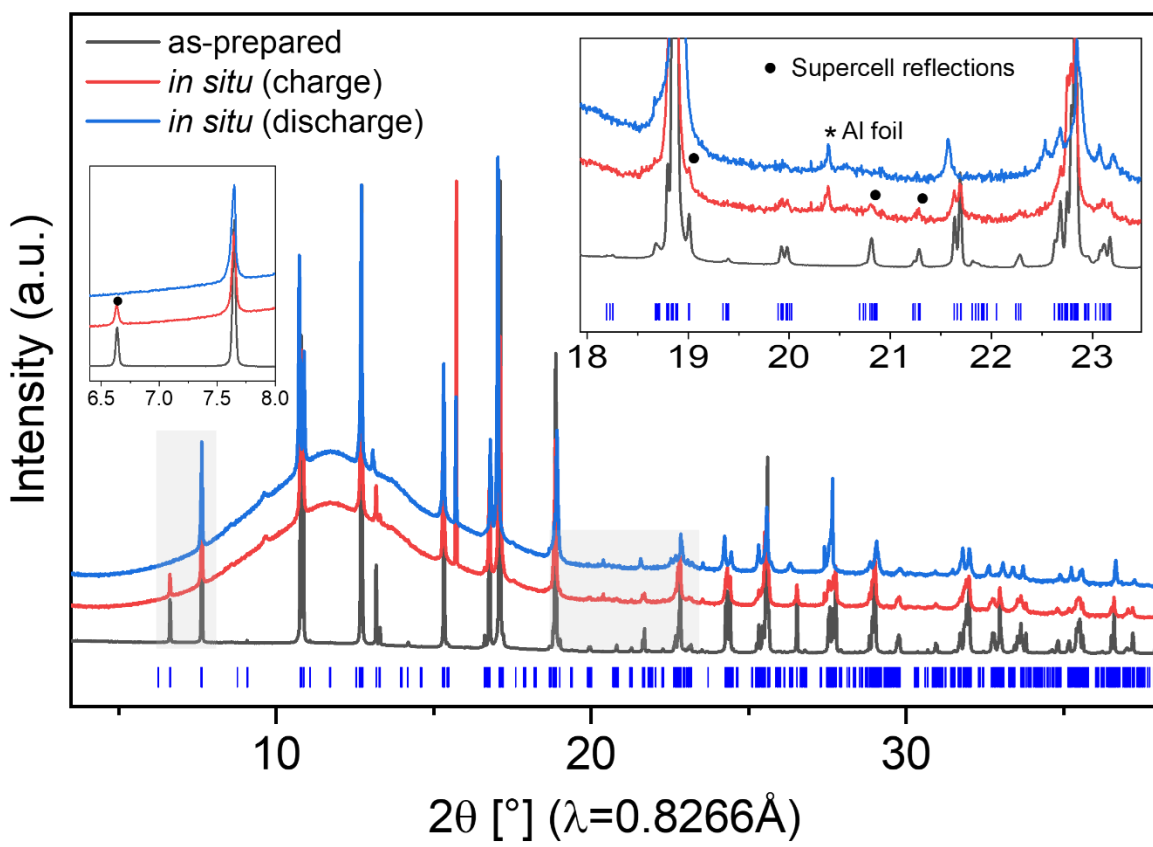


**Figure S8.** Comparison between the synchrotron XRPD patterns collected for  $\text{Na}_3\text{FeV}(\text{PO}_4)_3$  obtained by solid-state reaction at high temperature (black), and  $\text{Na}_3\text{FeV}(\text{PO}_4)_3$  obtained by  $\text{Na}^+$  de-intercalation(re-intercalation) from(in)  $\text{Na}_4\text{FeV}(\text{PO}_4)_3$  in the *in situ* cell during charge(discharge) (red(blue)). The XRPD pattern obtained in discharge (blue) shows the absence of the diffraction lines associated to the monoclinic distortion (as clearly observed at around  $6.6^\circ$ ).

**Table S1.** Refined structural parameters of the  $\text{Na}_4\text{FeV}(\text{PO}_4)_3$  from the synchrotron XRPD pattern collected with the *in situ* cell before cycling. Rietveld refinement profile is shown in Figure 2.

---

<b><math>\text{Na}_4\text{FeV}(\text{PO}_4)_3</math></b>						
Space group: $R\bar{3}c$ (#167); $Z=6$						
$a = 8.94160(9) \text{ \AA}$ ; $c = 21.3148(4) \text{ \AA}$ ; $c/a = 2.384$						
$V = 1475.85(3) \text{ \AA}^3$ ; $V/Z = 245.974(5) \text{ \AA}^3$						
$R_{wp} = 20.0 \%$ ; $R_p = 24.8 \%$ ; $R_{\text{Bragg}} = 12.5 \%$						
Atom	Wyckoff position	x/a	y/b	z/c	$U_{\text{iso}}, \text{\AA}^2$	Occ.
Fe/V(1)	12c	0	0	0.1482(3)	0.0088	0.5/0.5
P(1)	18e	0	0	0.1482(3)	0.0135	1
Na(1)	6b	0.2922(11)	0	0.25	0.0160	0.98(4)
Na(2)	18e	0	0	0	0.0170	0.938(15)
O(1)	36f	0.6373(16)	0	0.25	0.0180	1
O(2)	36f	0.020(2)	0.2046(18)	0.1933(7)	0.0160	1

---

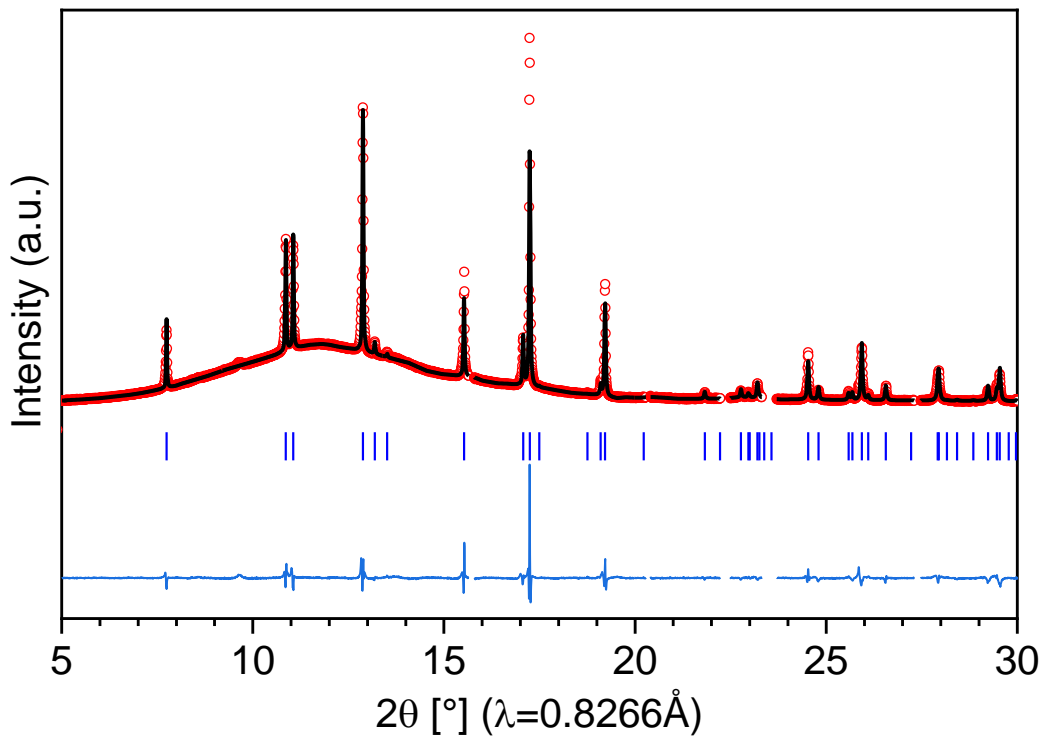


**Figure S9.** Rietveld refinement profile of the  $\text{Na}_2\text{FeV}(\text{PO}_4)_3$  from the synchrotron XRPD pattern collected with the *in situ* cell during charge.

**Table S2.** Refined structural parameters of the  $\text{Na}_2\text{FeV}(\text{PO}_4)_3$  from the synchrotron XRPD pattern collected with the *in situ* cell during charge.

### $\text{Na}_2\text{FeV}(\text{PO}_4)_3$

Space group:  $R-3c$  (#167);  $Z=6$

$a = 8.57794(11)$  Å;  $c = 21.5889(4)$  Å;  $c/a = 2.517$

$V = 1375.71(4)$  Å<sup>3</sup>;  $V/Z = 229.286(6)$  Å<sup>3</sup>

$R_{wp} = 21.5$  %;  $R_p = 25.4$  %;  $R_{Bragg} = 10.4$  %

Atom	Wyckoff position	x/a	y/b	z/c	Uiso, Å <sup>2</sup>	Occ.
Fe/V(1)	12c	0	0	0.1469(4)	0.0088	0.5/0.5
P(1)	18e	0	0	0.1469(4)	0.0135	1
Na(1)	6b	0.2895(13)	0	0.25	0.0160	0.98(4)
Na(2)	18e	0	0	0	0.0170	0.416(16)
O(1)	36f	0.644(5)	0	0.25	0.0180	1

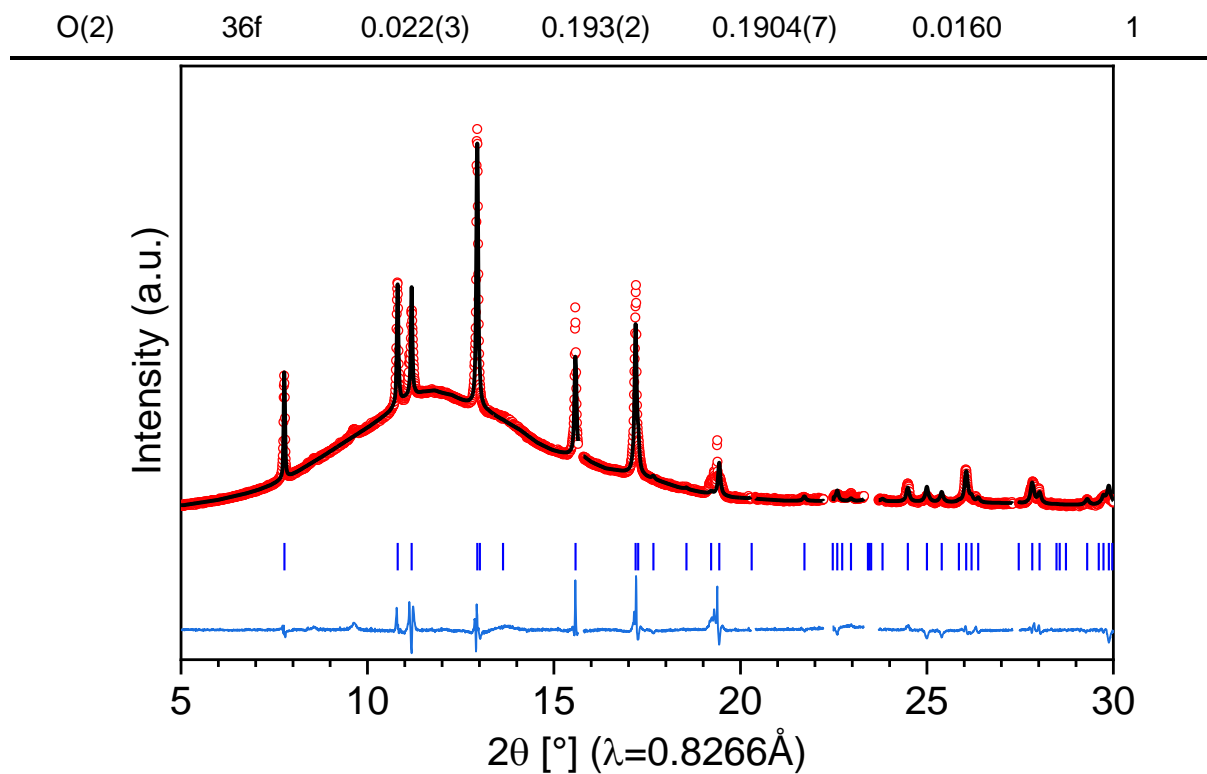


**Figure S10.** Rietveld refinement profile of the  $\text{Na}_{1.3}\text{FeV}(\text{PO}_4)_3$  from the synchrotron XRPD pattern collected with the *in situ* cell at the end of charge.

**Table S3.** Refined structural parameters of the  $\text{Na}_{1.3}\text{FeV}(\text{PO}_4)_3$  from the synchrotron XRPD pattern collected with the *in situ* cell at the end of charge.

**$\text{Na}_{1.3}\text{FeV}(\text{PO}_4)_3$**   
 Space group:  $R-3c$  (#167);  $Z=6$   
 $a = 8.4844(5) \text{\AA}$ ;  $c = 21.886(2) \text{\AA}$ ;  $c/a = 2.580$   
 $V = 1364.38(18) \text{\AA}^3$ ;  $V/Z = 227.396(5) \text{\AA}^3$   
 $R_{wp} = 27.3\%$ ;  $R_p = 37.8\%$ ;  $R_{\text{Bragg}} = 16.1\%$

Atom	Wyckoff position	x/a	y/b	z/c	Uiso, $\text{\AA}^2$	Occ.
Fe/V(1)	12c	0	0	0.1481(10)	0.0135	0.5/0.5
P(1)	18e	0	0	0.1481(10)	0.0276	1
Na(1)	6b	0.287(4)	0	0.25	0.0370	0.78(9)
Na(2)	18e	0	0	0	0.0370	0.18(6)
O(1)	36f	0.54(2)	0	0.25	0.0110	1

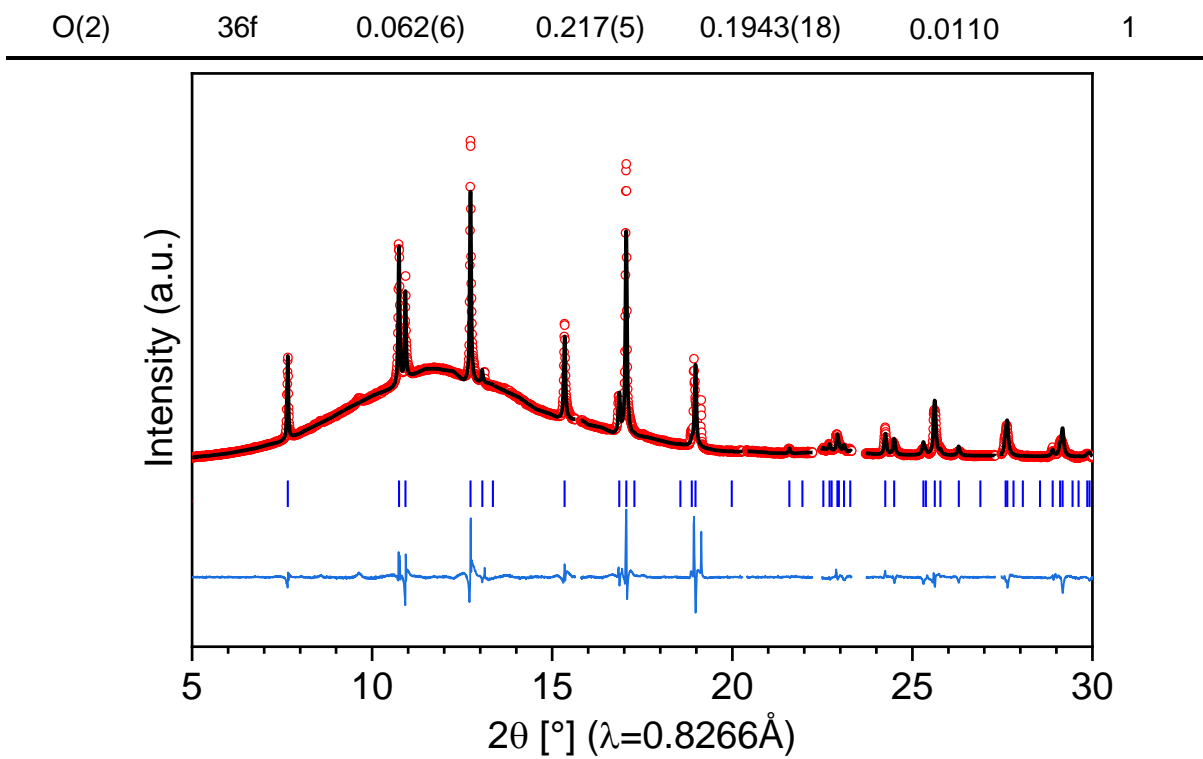


**Figure S11.** Rietveld refinement profile of the  $\text{Na}_{2.5}\text{FeV}(\text{PO}_4)_3$  from the synchrotron XRPD pattern collected with the *in situ* cell during discharge.

**Table S4.** Refined structural parameters of the  $\text{Na}_{2.5}\text{FeV}(\text{PO}_4)_3$  from the synchrotron XRPD pattern collected with the *in situ* cell during discharge.

**$\text{Na}_{2.5}\text{FeV}(\text{PO}_4)_3$**   
 Space group:  $R\bar{3}c$  (#167);  $Z=6$   
 $a = 8.6819(3)\text{\AA}$ ;  $c = 21.8170(10)\text{\AA}$ ;  $c/a = 2.513$   
 $V = 1424.15(9)\text{\AA}^3$ ;  $V/Z = 237.358(5)\text{\AA}^3$   
 $R_{wp} = 21.9\%$ ;  $R_p = 29.9\%$ ;  $R_{Bragg} = 12.9\%$

Atom	Wyckoff position	x/a	y/b	z/c	Uiso, $\text{\AA}^2$	Occ.
Fe/V(1)	12c	0	0	0.1484(6)	0.0102	0.5/0.5
P(1)	18e	0	0	0.1484(6)	0.0505	1
Na(1)	6b	0.301(2)	0	0.25	0.0403	0.91(5)
Na(2)	18e	0	0	0	0.0403	0.54(2)
O(1)	36f	0.650(6)	0	0.25	0.0234	1
O(2)	36f	0.034(4)	0.209(3)	0.1941(10)	0.0234	1

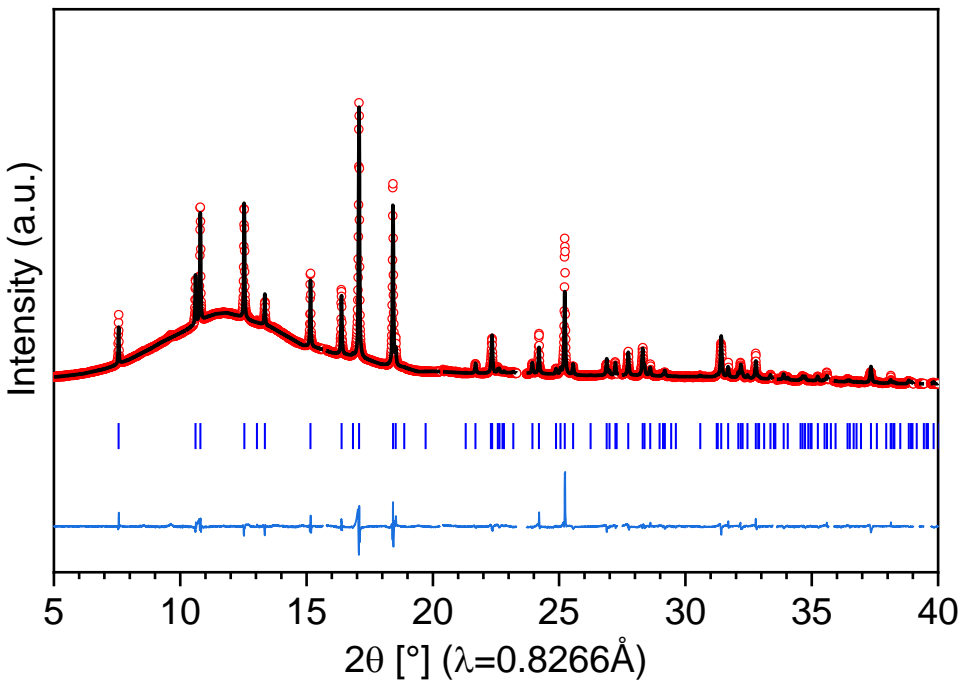


**Figure S12.** Rietveld refinement profile of the  $\text{Na}_4\text{FeV}(\text{PO}_4)_3$  from the synchrotron XRPD pattern collected with the *in situ* cell at the end discharge.

**Table S5.** Refined structural parameters of the  $\text{Na}_4\text{FeV}(\text{PO}_4)_3$  from the synchrotron XRPD pattern collected with the *in situ* cell at the end of discharge.

**$\text{Na}_4\text{FeV}(\text{PO}_4)_3$**   
 Space group:  $R\bar{3}c$  (#167);  $Z=6$   
 $a = 8.94445(10)$  Å;  $c = 21.3364(4)$  Å;  $c/a = 2.385$   
 $V = 1478.29(4)$  Å<sup>3</sup>;  $V/Z = 246.382(5)$  Å<sup>3</sup>  
 $R_{wp} = 20.5\%$ ;  $R_p = 25.5\%$ ;  $R_{Bragg} = 10.9\%$

Atom	Wyckoff position	x/a	y/b	z/c	Uiso, Å <sup>2</sup>	Occ.
Fe/V(1)	12c	0	0	0.1493(3)	0.0201	0.5/0.5
P(1)	18e	0	0	0.1493(3)	0.0408	1
Na(1)	6b	0.2959(12)	0	0.25	0.0283	0.89(4)
Na(2)	18e	0	0	0	0.0283	0.984(16)
O(1)	36f	0.648(2)	0	0.25	0.0323	1
O(2)	36f	0.025(2)	0.214(2)	0.1929(7)	0.0323	1

**Table S6.** Room temperature  $^{57}\text{Fe}$  Mössbauer refined parameters (isomer shift ( $\delta$ ), quadrupole splitting ( $\Delta$ ), Full-Width at Half-Maximum ( $\Gamma$ ) and Relative Area (%)) extracted from the analysis of spectra collected *ex situ* for  $\text{Na}_x\text{FeV}(\text{PO}_4)_3$  compounds obtained at different states of charge or discharge.

x in $\text{Na}_x\text{FeV}(\text{PO}_4)_3$	Voltage	Site	$\delta$ (mm/s)	$\Delta$ (mm/s)	$\Gamma$ (mm/s)	Rel. Area (%)
4.0	OCV	$\text{Fe}^{3+}(\text{I})$	0.47(2)	0.50(2)	0.38(2)	13(3)
		$\text{Fe}^{2+}$	1.24(1)	2.25(2)	0.38(1)	87(3)
3.0	3.4 V	$\text{Fe}^{3+}(\text{I})$	0.44(1)	0.33(2)	0.27(1)	87(3)
		$\text{Fe}^{3+}(\text{II})$	0.38(2)	0.79(5)	0.46(4)	13(3)
2.0	3.75 V	$\text{Fe}^{3+}(\text{I})$	0.44(1)	0.36(2)	0.39(2)	85(3)
		$\text{Fe}^{3+}(\text{II})$	0.36(2)	0.86(6)	0.45(5)	15(3)
1.3	4.3 V	$\text{Fe}^{3+}(\text{I})$	0.43(1)	0.51(3)	0.39(2)	66(3)
		$\text{Fe}^{3+}(\text{II})$	0.39(2)	1.08(5)	0.39(2)	34(3)
2.4	3.15 V	$\text{Fe}^{3+}(\text{I})$	0.44(1)	0.35(2)	0.32(2)	74(3)
		$\text{Fe}^{3+}(\text{II})$	0.38(2)	0.88(6)	0.44(4)	26(3)
3.3	2.0 V	$\text{Fe}^{3+}(\text{I})$	0.46(2)	0.42(3)	0.33(2)	46(3)
		$\text{Fe}^{2+}$	1.20(2)	2.15(4)	0.49(4)	54(3)
3.7	1.3 V	$\text{Fe}^{3+}(\text{I})$	0.42(3)	0.41(3)	0.41(3)	25(3)
		$\text{Fe}^{2+}$	1.24(2)	2.23(4)	0.41(3)	75(3)

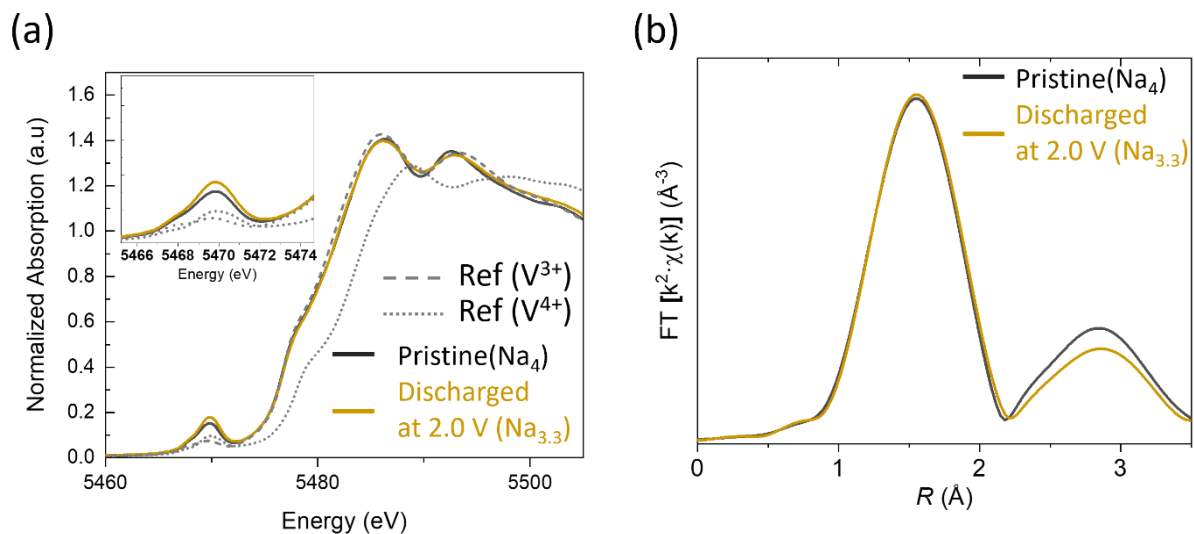


**Figure S13** (a) Comparison of XANES spectra of V K-edge obtained before and after cycling (b) corresponding  $k^2$ -weighted Fourier transformed EXAFS oscillations of V K-edge obtained before and after cycling. References for V K-edge XAS spectra:  $V^{3+}$  ( $Na_3V_2(PO_4)_3$ ) and  $V^{4+}$  ( $Na_1V_2(PO_4)_3$ ).

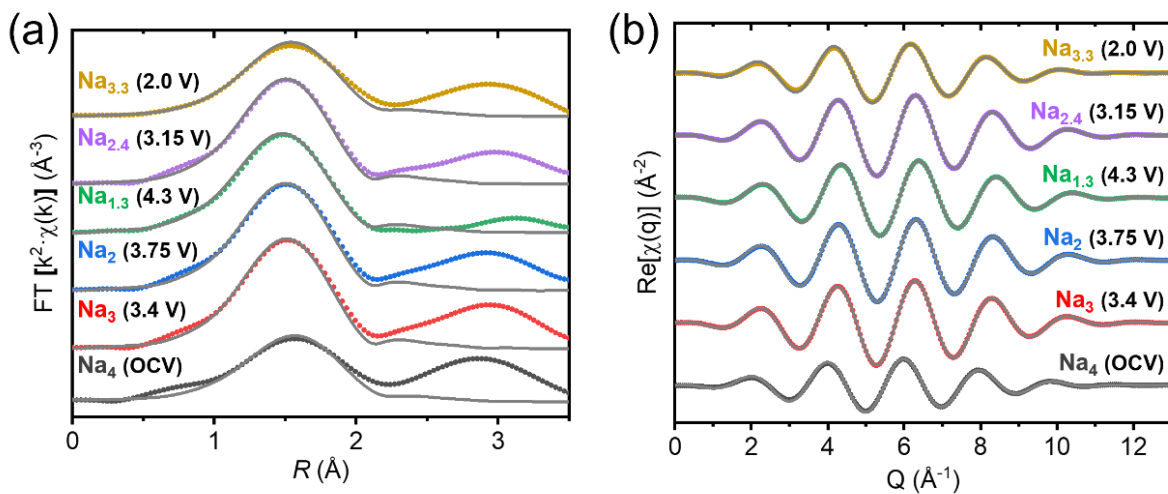


**Figure S14** (a)  $k^2$ -weighted Fourier transformed EXAFS oscillations of Fe K-edge for  $\text{Na}_x\text{FeV}(\text{PO}_4)_3$  compounds recovered at different states of charge or discharge of the battery. (b) Corresponding backward Fourier transforms in  $q$ -space.

**Table S7.** Refined parameters for the first shell of Fe K-edge EXAFS spectra.  $k$ -range: 2.6 - 10.8 Å<sup>-1</sup>, R-range: 1.0 - 2.1 Å, dR = 0, sine window. The coordination number (N) was set to 6, and attenuation factors ( $S_0^{-2}$ ) were fixed as 0.95. The Fe – O distances and the Debye-Waller factors ( $\sigma_i^2$ ) were refined, whereas the energy shift ( $E_0$ ) was first refined before being fixed.

x in $\text{Na}_x\text{FeV}(\text{PO}_4)_3$	Voltage	CN	d(Fe – O) (Å)	$E_0$ (eV)	$\sigma^2$ (Å <sup>2</sup> )	R-factor
4	OCV	6	2.067(5)	0.0	0.0121(5)	0.0092
3	3.4 V	6	1.987(5)	0.2	0.0070(5)	0.0024
2	3.75 V	6	1.981(5)	0.1	0.0074(5)	0.0017
1.3	4.3 V	6	1.964(5)	0.0	0.0086(5)	0.0031
2.4	3.15 V	6	1.983(5)	0.1	0.0076(5)	0.0015
3.3	2.0 V	6	2.031(5)	1.9	0.0117(5)	0.0120

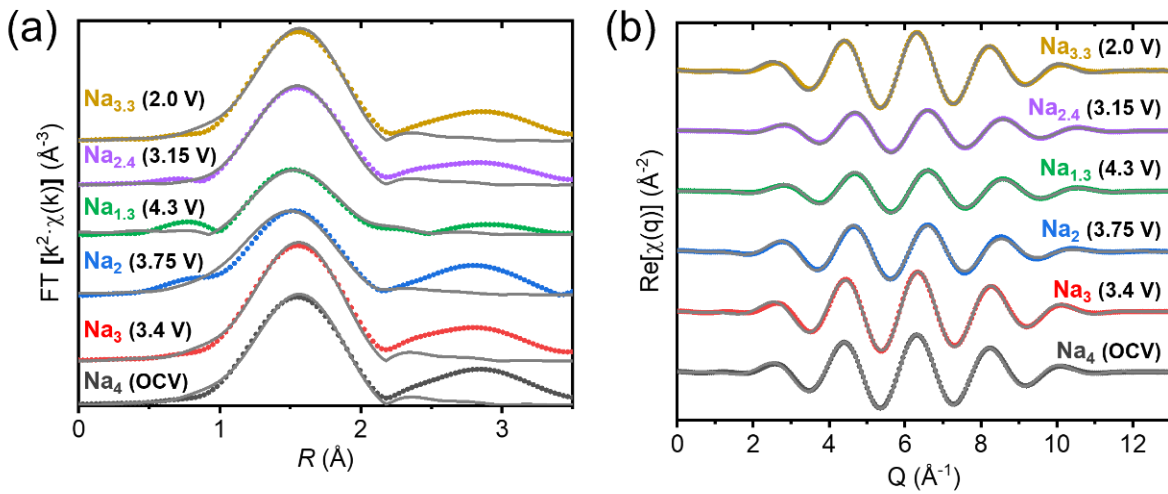


**Figure S15.** (a)  $k^2$ -weighted Fourier transformed EXAFS oscillations of V K-edge for  $\text{Na}_x\text{FeV}(\text{PO}_4)_3$  compounds recovered at different states of charge or discharge of the battery. (b) Corresponding backward Fourier transforms in  $q$ -space.

**Table S8** Refined parameters for the first shell of V K-edge EXAFS spectra.  $k$ -range: 2.7 - 10.7  $\text{\AA}^{-1}$ ,  $R$ -range: 1.0 - 2.2  $\text{\AA}$ ,  $dR = 0$ , sine window. The coordination number (N) was set to 6, and attenuation factors ( $S_0^2$ ) were fixed as 0.7. The V – O distances and the Debye-Waller factors ( $\sigma_i^2$ ) were refined, whereas the energy shift ( $E_0$ ) was first refined before being fixed.

x in $\text{Na}_x\text{FeV}(\text{PO}_4)_3$	Voltage	CN	$d(\text{V} - \text{O}) (\text{\AA})$	$E_0 (\text{eV})$	$\sigma^2 (\text{\AA}^2)$	R-factor
4	OCV	6	2.029(5)	-0.2	0.0038(5)	0.0089
3	3.4 V	6	2.022(5)	0.0	0.0031(5)	0.0087
2	3.75 V	6	1.968(5)	1.2	0.0082(5)	0.0121
1.3	4.3 V	5	1.949(5)	0.1	0.0071(5)	0.0086
		1	1.648(5)			
2.4	3.15 V	5.5	2.012(5)	0.1	0.0042(5)	0.0046
		0.5	1.657(5)			
3.3	2.0 V	6	2.030(5)	-0.1	0.0036(5)	0.0115

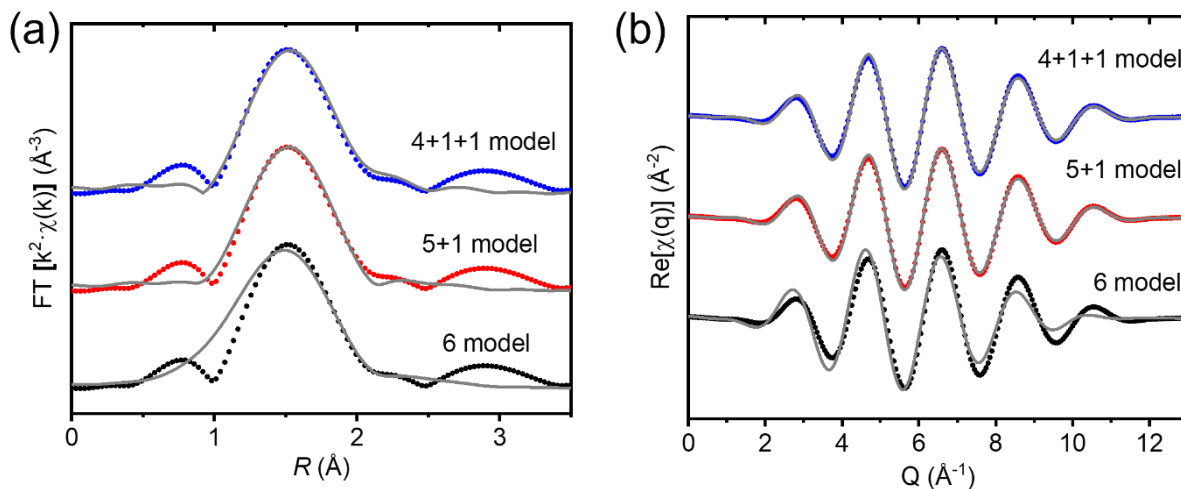


**Figure S16.** (a) Different coordination models of  $k^2$ -weighted Fourier transformed EXAFS oscillations at V K-edge at the end of charge at 4.3 V. (b) Corresponding backward Fourier transforms in  $q$ -space.

**Table S9** Refined parameters for the first shell of V K-edge EXAFS spectra considering different coordination models for V in  $\text{Na}_x\text{FeV}(\text{PO}_4)_3$  recovered at 4.3 V.  
 $k$ -range:  $2.7 - 10.7 \text{\AA}^{-1}$ ,  $R$ -range:  $1.0 - 2.2 \text{\AA}$ ,  $dR = 0$ , sine window

Coordination model	$d(\text{V} - \text{O}) (\text{\AA})$	$E_0 (\text{eV})$	$\sigma^2 (\text{\AA}^2)$	R-factor
6	$1.967(5) \times 6$	1.1	$0.0117(5)$	0.1248
5+1	$1.949(5) \times 5$	0.1	$0.0071(5)$	0.0086
	$1.648(5) \times 1$			
4+1+1	$1.938(5) \times 4$	-0.1	$0.0048(5)$	0.0036
	$1.640(5) \times 1$			
	$2.531(5) \times 1$			

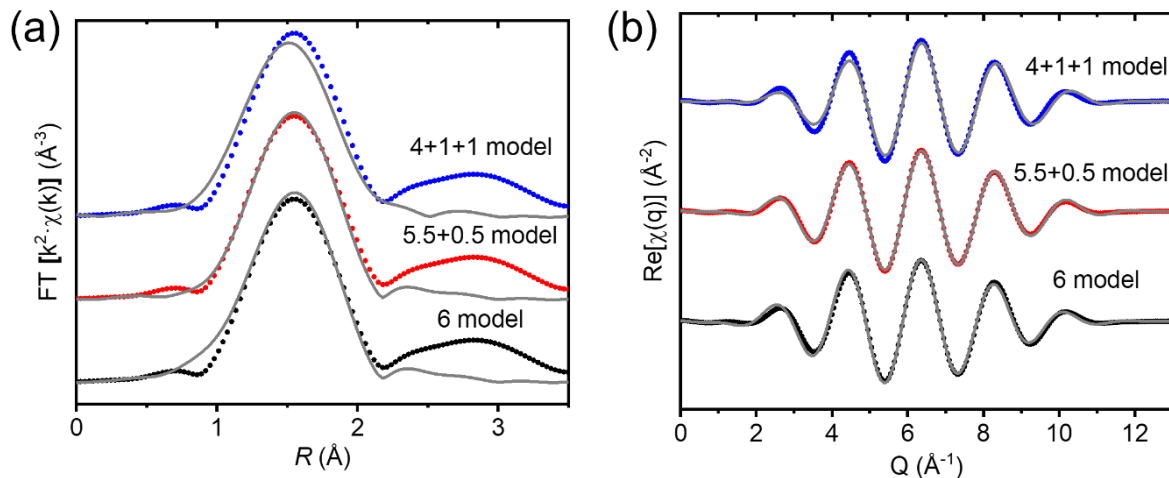


**Figure S17.** (a) Different coordination models of  $k^2$ -weighted Fourier transformed EXAFS oscillations at V K-edge after the first discharge domain at 3.15 V. (b) Corresponding backward Fourier transforms in  $q$ -space.

**Table S10** Refined parameters for the first shell of V K-edge EXAFS spectra considering different coordination models for V in  $\text{Na}_x\text{FeV}(\text{PO}_4)_3$  recovered at 3.15 V. k-range: 2.7 - 10.7  $\text{\AA}^{-1}$ , R-range: 1.0 - 2.2  $\text{\AA}$ , dR = 0, sine window

Coordination model	d(V – O) ( $\text{\AA}$ )	$E_0$ (eV)	$\sigma^2$ ( $\text{\AA}^2$ )	R-factor
6	2.019(5) X 6	-0.1	0.0050(5)	0.0220
5.5+0.5	2.012(5) X 5.5	0.1	0.0042(5)	0.0046
	1.657(5) X 0.5			
	1.997(5) X 4			
4+1+1	1.622(5) X 1	0.0	0.0028(5)	0.0338
	2.552(5) X 1			